

## Coordination Chemistry at the Molybdenum Site of Sulfite Oxidase: Redox-Induced Structural Changes in the Cysteine 207 to Serine Mutant

Graham N. George,<sup>\*†</sup> Robert M. Garrett,<sup>‡</sup> Roger C. Prince,<sup>§</sup> and K. V. Rajagopalan<sup>‡</sup>

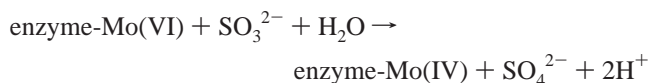
Department of Geological Sciences, University of Saskatchewan, Saskatoon, Saskatchewan S7N 5E2, Canada, Department of Biochemistry, School of Medicine, Duke University, Durham, North Carolina 27710, and ExxonMobil Research and Engineering Company, Annandale, New Jersey 08801

Received July 27, 2004

The redox chemistry of the molybdenum site of the C207S mutant of recombinant human sulfite oxidase has been studied via potentiometric titrations employing both electron paramagnetic resonance (EPR) spectroscopy and X-ray absorption spectroscopy (XAS) as probes of the active site structure. In earlier EXAFS studies, oxidized Cys207Ser enzyme has been shown to possess a novel tri-oxo active site, in which Ser207 does not appear to be a ligand to Mo [George, G. N.; Garrett, R. M.; Prince, R. C.; Rajagopalan, K. V. *J. Am. Chem. Soc.* **1996**, *118*, 8588–8592]. Redox titrations show that the active site is modified under reducing conditions to a mono-oxo Mo(IV) species, probably with Ser207 ligated to the metal. The Mo(IV) species can be reoxidized to a mono-oxo Mo(V) species still coordinated to Ser207, which in turn can be further reoxidized to yield the initial tri-oxo Mo(VI) structure with loss of Ser207 ligation.

### Introduction

Sulfite oxidase (SO) is an oxo-transferase enzyme responsible for the physiologically vital oxidation of sulfite to sulfate.<sup>1</sup> Residing in the mitochondrial intermembrane space, the enzyme is dimeric with a subunit mass of about 52 000. Each monomer contains molybdenum associated with a single pterin cofactor, and a cytochrome *b* type heme. The two-electron oxidation of sulfite to sulfate is known to occur at the molybdenum site, which is reduced from Mo(VI) to Mo(IV) in the process. The catalytic cycle is completed with reoxidation of the molybdenum first to Mo(V), and then to Mo(VI), by intramolecular electron transfer to the cytochrome *b* site, with cytochrome *c* serving as the external electron acceptor.<sup>2,3</sup>



With the exception of nitrogenase, all molybdenum enzymes that have been described to date contain a novel pyranopterin-dithiolene cofactor (known as molybdopterin) in which the molybdenum is coordinated by the dithiolene moiety.<sup>4,5</sup> The crystal structure of chicken SO confirms that the active site is coordinated by one dithiolene, with two terminal oxygen atoms and one additional sulfur ligand from

\* Author to whom correspondence should be addressed. Phone: 306-966-5722. Fax: 306-966-8593. E-mail: g.george@usask.ca.

† University of Saskatchewan.

‡ Duke University Medical Center.

§ ExxonMobil Research and Engineering.

- (1) (a) McLeod, R. M.; Farkas, W.; Fridovitch, I.; Handler, P. *J. Biol. Chem.* **1961**, *236*, 1841–1852. (b) Cohen, H. L.; Betcher-Lange, S.; Kessler, D. L.; Rajagopalan, K. V. *J. Biol. Chem.* **1972**, *247*, 7759–7766.
- (2) Johnson, J. L.; Rajagopalan, K. V. *J. Biol. Chem.* **1977**, *252*, 2017–2025.
- (3) Elliot, S. J.; McElhaney, A. E.; Feng, C.; Enemark, J. H.; Armstrong, F. *J. Am. Chem. Soc.* **2002**, *124*, 11612–11613.

- (4) (a) Rajagopalan, K. V. *Adv. Enzymol. Relat. Areas Mol. Biol.* **1991**, *64*, 215–290. (b) Rajagopalan, K. V.; Johnson, J. L. *J. Biol. Chem.* **1992**, *267*, 10199–10202.

- (5) Molybdenum enzymes have previously been described as all involving two-electron redox chemistry at molybdenum, coupled with the transfer of an oxygen atom. While this is true for the majority of molybdenum enzymes (and for their close relatives, the tungsten enzymes), there are some exceptions. The tungsten enzyme acetylene hydratase [Rosner, B. M.; Schink, B. *J. Bacteriol.* **1995**, *177*, 5767–5772] catalyzes a net hydration reaction rather than a redox one, and formate oxidation to CO<sub>2</sub> by *Escherichia coli* formate dehydrogenase H does not involve oxygen atom transfer [Khangulov, S. V.; Gladyshev, V. N.; Dismukes, G. C.; Stadtman, T. C. *Biochemistry* **1998**, *37*, 3518–3528]. Furthermore, the presence of the potentially redox-active seleno-sulfide at the active site [George, G. N.; Colangelo, C. M.; Dong, J.; Scott, R. A.; Khangulov, S. V.; Gladyshev, V. N.; Stadtman, T. C. *J. Am. Chem. Soc.* **1998**, *120*, 1267–1273] suggests that the molybdenum in formate dehydrogenases might not be redox active during the catalysis [George, G. N.; Costa, C.; Moura, J. J. G.; Moura, I. *J. Am. Chem. Soc.* **1999**, *121*, 2625–2626].

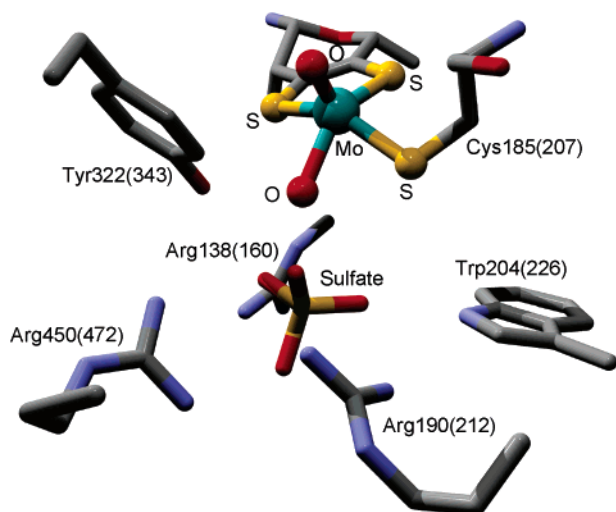


**Figure 1.** Crystal structure of chicken sulfite oxidase active site,<sup>6</sup> showing several important active site amino acids. The numbering scheme for amino acids is that of the chicken enzyme with that of the human enzyme given in parentheses.

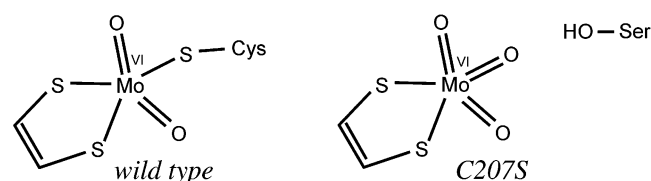


**Figure 2.** Active site structures for oxidized wild-type and C207S mutant sulfite oxidase.

cysteine 185 (Cys207 in human SO) (Figure 1).<sup>6</sup> As one of the most intensively studied molybdenum enzymes, SO can be regarded as the prototypical member of one family of molybdenum enzymes<sup>7</sup> possessing di-oxo molybdenum sites when the enzyme is in the fully oxidized Mo(VI) form.

In earlier EXAFS studies, we examined the properties of the Cys207 → Ser mutant (C207S) of human SO and showed that the oxidized active site is a novel tri-oxo species in which Ser207 is not coordinated (Figure 2).<sup>8</sup> In these experiments, the C207S enzyme was found to be very resistant to reduction by solutions of sodium dithionite. We present herein an X-ray absorption spectroscopy (XAS) and electron paramagnetic resonance (EPR) spectroscopic study of the redox chemistry of this novel form of SO. Our results suggest that the coordination of Ser207 is labile in that it can become ligated to Mo upon reduction to the Mo(IV) oxidation state, but dissociates again upon reoxidation to Mo(VI).

## Materials and Methods

**Sample Preparation.** Recombinant human SO was obtained as described by Garrett and Rajagopalan.<sup>9</sup> Samples for XAS and EPR were prepared in a mixed buffer system consisting of 20 mM Tris, bis-Tris, and bis-Tris-propane pH 6.0, with chloride rigorously

excluded from the solutions, except where otherwise stated. For molybdenum K-edge XAS measurements, samples at approximately 0.3 mM Mo were frozen in 10 mm × 10 mm × 2 mm Lucite sample cuvettes. For EPR measurements, samples at approximately 0.1 mM Mo were quickly frozen in 3 mm internal diameter quartz tubes by immersion in a bath of cold (−140 °C) isopentane.

**XAS Data Collection.** XAS measurements were carried out at the Stanford Synchrotron Radiation Laboratory with the SPEAR storage ring containing 55–90 mA at 3.0 GeV. Molybdenum K-edge data were collected on beamline 7-3 using a Si(220) double crystal monochromator, with an upstream vertical aperture of 1 mm, and a wiggler field of 1.8 T. Harmonic rejection was accomplished by detuning one monochromator crystal to approximately 50% off peak, and no specular optics were present in the beamline. The incident X-ray intensity was monitored using an argon-filled ionization chamber, and X-ray absorption was measured as the X-ray Mo K $\alpha$  fluorescence excitation spectrum using either a 13-element or a 30-element germanium array detector.<sup>10</sup> Samples were maintained at a temperature of approximately 10 K during data collection using an Oxford Instruments liquid helium flow cryostat. Eight 35-min scans were accumulated for each sample, and the absorption of a molybdenum metal foil was measured simultaneously by transmittance. The X-ray energy was calibrated with reference to the lowest energy inflection point of the foil spectrum, which was assumed to be 20 003.9 eV.

**Data Analysis.** The extended X-ray absorption fine structure (EXAFS) oscillations  $\chi(k)$  were quantitatively analyzed by curve-fitting with the EXAFSPAK suite of computer programs<sup>11</sup> using ab initio theoretical phase, amplitude, and mean free path functions generated with the program FEFF version 7.2.<sup>12</sup> No smoothing or related manipulation was performed upon the data.

**EPR Spectroscopy.** Electron paramagnetic resonance (EPR) spectroscopy, data reduction, and spectral simulations were performed as described by George et al.<sup>13</sup> Redox titrations followed the method of Dutton<sup>14</sup> using 40  $\mu$ M *N*-methylphenazonium methosulfate, *N*-ethylphenazonium ethosulfate, 2-hydroxy-1,4-naphthoquinone, 2-hydroxy-1,4-anthraquinone, indigo disulfonate, indigo trisulfonate, and benzyl viologen as redox mediators between the protein and the platinum measuring electrode. Potentials were measured with respect to a saturated calomel electrode, but are reported with respect to the hydrogen electrode by assuming that the calomel electrode has a potential of +247 mV.<sup>15</sup>

## Results and Discussion

The addition of buffered solutions of sodium dithionite is generally used as an effective method for the reduction of molybdenum enzymes, but the C207S mutant of human SO does not become reduced at all by 10 mM sodium dithionite (as judged by changes in the X-ray absorption near-edge spectrum). Preliminary experiments using both dithionite and mediator dyes showed some reduction at low pH. We

(6) Kisker, C.; Schindelin, H.; Pacheco, A.; Wehbi, W. A.; Garrett, R. M.; Rajagopalan, K. V.; Enemark, J. E.; Rees, D. C. *Cell* **1997**, *91*, 1–20.

(7) Hille, R. *Chem. Rev.* **1996**, *96*, 2757–2816.

(8) George, G. N.; Garrett, R. M.; Prince, R. C.; Rajagopalan, K. V. *J. Am. Chem. Soc.* **1996**, *118*, 8588–8592.

(9) Garrett, R. M.; Rajagopalan, K. V. *J. Biol. Chem.* **1996**, *271*, 7387–7391.

(10) Cramer, S. P.; Tench, O.; Yocum, M.; George, G. N. *Nucl. Instrum. Methods Phys. Res.* **1988**, *A266*, 586–591.

(11) The EXAFSPAK program suite was developed by G.N.G. and is available from <http://ssrl.slac.stanford.edu/exafspak.html>.

(12) (a) Rehr, J. J.; Mustre de Leon, J.; Zabinsky, S. I.; Albers, R. C. *J. Am. Chem. Soc.* **1991**, *113*, 5135–5140. (b) Mustre de Leon, J.; Rehr, J. J.; Zabinsky, S. I.; Albers, R. C. *Phys. Rev.* **1991**, *B44*, 4146–4156.

(13) George, G. N.; Prince, R. C.; Kipke, C. A.; Sunde, R. A.; Enemark, J. H. *Biochem. J.* **1988**, *256*, 307–309.

(14) Dutton, P. L. *Methods Enzymol.* **1978**, *24*, 431–446.

(15) Clark, W. M. *Oxidation–Reduction Potentials of Organic Systems*; Williams and Wilkins: Baltimore, MD, 1960.

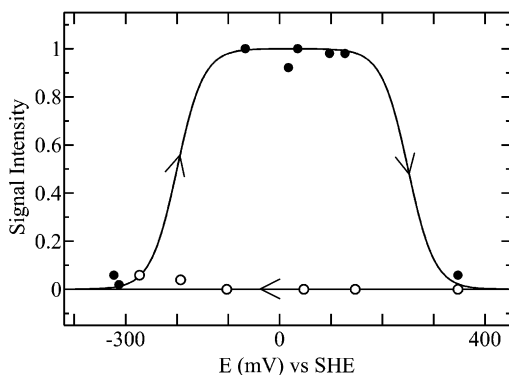


**Figure 3.** EPR redox titration of C207S sulfite oxidase. The EPR signal intensity is plotted as a function of the potential. The data points for the reductive part of the redox titration are shown as ○, while those of the oxidative part are shown as ●. The solid lines are drawn to guide the eye.

therefore attempted to reduce the molybdenum site of the enzyme by using redox potentiometry at pH 6.0, with monitoring for Mo(V) EPR signal intensity, starting with fully oxidized, as-isolated, enzyme. The results of this experiment are shown in Figure 3. During the reductive part of the titration, no Mo(V) EPR signal was observed at all, suggesting that the Mo(V)/Mo(IV) midpoint potential is much more positive than the Mo(VI)/Mo(V) couple. However, on raising the potential above its lowest point of about  $-320$  mV, intense Mo(V) EPR signals were observed between  $-100$  and  $+150$  mV (Figure 4c). The Mo(V) EPR signal of the C207S mutant is unusually isotropic with  $\Delta g = (g_{zz} - g_{xx}) = 0.0244$ , and has significantly lower  $g$ -values than both of the commonly designated EPR signals of SO (the so-called low-pH/Cl<sup>-</sup> and high-pH signals, Figure 4a and b);  $g_{ave} = 1.9663$  versus 1.9806 and 1.9675 for low-pH/Cl<sup>-</sup> and high-pH wild-type SO signals, respectively. We note that the difference in  $g_{ave}$  values between the high-pH and C207S EPR signals is smaller than that between high-pH and low-pH/Cl<sup>-</sup> signals. Reduction of a tri-oxo Mo(VI) species by one electron to Mo(V) might be expected to yield a *cis*-dioxo Mo(V) species, with one of the three original Mo=O groups becoming protonated to Mo–OH. Mo(V) EPR signals from *cis*-dioxo species are well-known<sup>16</sup> and typically have low  $g$ -values with remarkably high  $g$ -anisotropy, for example,<sup>16</sup>  $g_{ave} = 1.901$  and  $\Delta g = 0.173$ . Thus, the possibility that the C207S Mo(V) EPR signal arises from a *cis*-dioxo species can be reasonably excluded from the  $g$ -values alone.

Both high-pH and low-pH/Cl<sup>-</sup> Mo(V) signals from wild-type SO show hyperfine coupling to an exchangeable proton. In the case of the low-pH/Cl<sup>-</sup> signal, the coupled proton results in a resolved splitting of the features of the EPR signal.<sup>17</sup> In contrast, with the high-pH signal, magic angle effects mean that no splitting is observed. However, the presence of a strongly coupled proton was revealed by the observation of formally forbidden  $\Delta M_I = \pm 1$  transitions

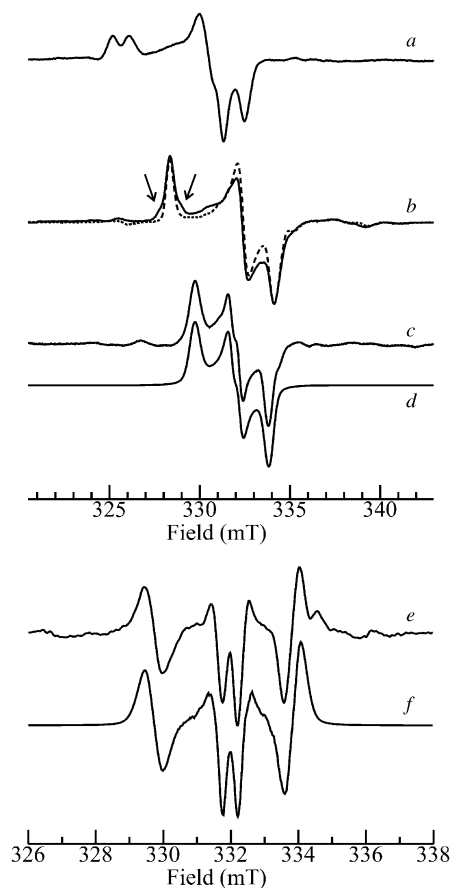


**Figure 4.** Mo(V) EPR signals from wild-type and C207S sulfite oxidase. (a) Low-pH/Cl<sup>-</sup> signal (pH 6.0, 1 M KCl), (b) high-pH signal (pH 9.0) (in <sup>1</sup>H<sub>2</sub>O, solid line, and in <sup>2</sup>H<sub>2</sub>O, with the proton spin-flip lines indicated by arrows), (c) C207S signal (pH 6.0), and (d) a computer simulation of (c) using  $g_{(xx,yy,zz)} = 1.9545, 1.9654, 1.9789$ , assuming hyperfine coupling to an  $I = 1/2$  nucleus  $A_{(xx,yy,zz)} = 6, 12, 6$  MHz (note that  $A_{xx}$  and  $A_{zz}$  are unresolved). The splitting of the C207S EPR signal is clearly shown in the second derivative EPR spectrum (e), and the corresponding simulation (f). All spectra are aligned to a microwave frequency of 9.13208 GHz.

(proton spin-flip lines)<sup>18</sup> and was later confirmed and quantitatively extended by pulsed EPR methods.<sup>19</sup>

The C207S SO EPR signal shows the expected satellite lines due to  $I = 5/2$  <sup>95</sup>Mo and <sup>97</sup>Mo isotopes (not illustrated)<sup>20</sup> and a few other signs of hyperfine structure. The central  $g_{yy}$  feature appears to be split into two, and this is modeled well by a hyperfine splitting of 12 MHz, which might suggest a coupled proton. The C207S SO EPR signal did not change when the redox titration was performed in deuterated buffer, indicating that if this structure is due to a coupled proton (which seems likely) then it is not exchangeable under our experimental conditions. The addition of anions, such as chloride and phosphate, modified the signal (not illustrated); chloride produced subtle  $g$ -value shifts and a distinct broadening of the line widths (possibly due to unresolved coupling to  $I = 3/2$  <sup>35</sup>Cl and <sup>37</sup>Cl), while phosphate produced a significantly modified signal, with shifts in  $g$ -values and possibly <sup>31</sup>P hyperfine coupling, indicating that the active site is still capable of interacting with anions.<sup>13,21,22</sup>

(16) Dowerah, D.; Spence, J. T.; Singh, R.; Wedd, A. G.; Wilson, G. L.; Farchione, F.; Enemark, J. H.; Kristofzski, J.; Bruck, M. *J. Am. Chem. Soc.* **1987**, *109*, 5655–5665.

(17) Lamy, M. T.; Gutteridge, S.; Bray, R. C. *Biochem. J.* **1980**, *185*, 397–403.

(18) George, G. N. *J. Magn. Reson.* **1985**, *64*, 384–394.

(19) Astashkin, A. V.; Mader, M. L.; Pacheco, A.; Enemark, J. H.; Raitsimring, A. M. *J. Am. Chem. Soc.* **2000**, *122*, 5294–5302.

(20) George, G. N.; Bray, R. C. *Biochemistry* **1988**, *27*, 3603–3609.

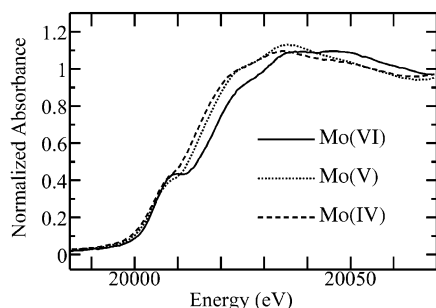


**Figure 5.** Mo K X-ray absorption near-edge spectra of C207S sulfite oxidase in the Mo(VI), Mo(V), and Mo(IV) oxidation states.

More quantitative information on active site structure is available from X-ray absorption spectroscopy. The Mo(V) EPR signal of the C207S mutant typically integrated to close to 100% Mo(V), and so XAS is well suited to a direct determination of the coordination of the Mo(V) EPR signal-giving species. Figure 5 shows the Mo K near-edge spectra of three different redox states of C207S sulfite oxidase. The spectrum of the fully oxidized Mo(VI) enzyme is essentially identical to that reported earlier, as is our analysis of the data.<sup>9</sup> As was previously discussed,<sup>9</sup> the Mo=O bond lengths (1.75 Å) are consistent with a tri-oxo site, and the Mo–S bond lengths (2.48 Å) are only slightly longer than normal, suggesting that the active site geometry of the oxidized C207S mutant is such that any oxo trans effects are small. The reduced forms were made by lowering the potential to –330 mV, generating the Mo(IV) species, and then raising it to +33 mV, where the Mo(V) species is predominant. Clear shifts to lower energy from Mo(VI) to Mo(V) to Mo(IV) can be seen (Figure 5), which are expected for the assigned oxidation states. Figure 6 shows the EXAFS oscillations and the corresponding EXAFS Fourier transforms (phase-corrected for Mo–S backscattering), together with the results of EXAFS curve-fitting analysis, which yielded structural parameters that are summarized in Table 1. The curve-fitting confirms our previous analysis<sup>8</sup> and shows that the oxidized enzyme has a novel tri-oxo coordination. In contrast, both Mo(V) and Mo(IV) forms of C207S sulfite oxidase have mono-oxo active sites (common for molybdenum compounds with these formal oxidation states), along with two equivalent Mo–S interactions from the cofactor, and approximately two interactions with oxygen-like ligands.<sup>23</sup> The Mo(V) form fits best with two equivalent Mo–O interactions at 1.94 Å, while the Mo(IV) form fits best with two different interactions Mo–O at 2.05 and 2.18 Å, respectively. This relative increase in Mo–O bond length is consistent with increased protonation of an oxygen at the lower oxidation state, that is, Mo(V)–OH and Mo(IV)–OH<sub>2</sub> species (Figure 7). The Mo(V)–OH proton could be responsible for the observed hyperfine structure in the Mo(V) EPR signal discussed above.

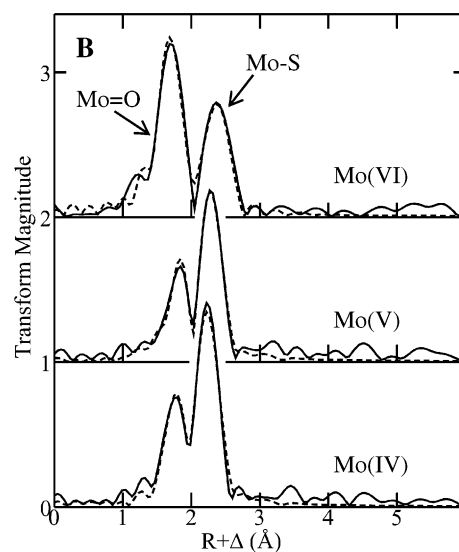
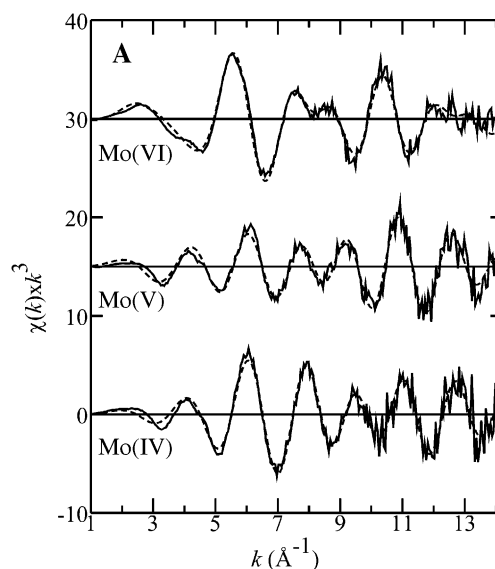


**Figure 6.** Mo K-edge EXAFS spectra (A) and Mo–S phase-corrected Fourier transforms (B) of C207S sulfite oxidase in the Mo(VI), Mo(V), and Mo(IV) oxidation states. Solid lines show experimental data, and broken lines represent the best fits.

The results of the redox titration were unusual, because the Mo(V) state was not observed at all during the reductive half of the titration but was quantitatively formed during the subsequent oxidative half. These findings lead to the conclusion that the coordination environment of the active site undergoes chemical modification at low potential that facilitates access to the reduced Mo(V) as well as Mo(IV) oxidation states. A likely possibility is that the hydroxyl of Serine 207, which is likely to be in close proximity to the active site, becomes ligated to the molybdenum under highly reducing conditions. This species might then be oxidized to a stable Mo(V) entity, which gives rise to the EPR signal of Figure 4. This hypothesis might be tested by constructing and examining C207 mutants involving other residues incapable of coordinating metal (such as C207A), and this will be the subject of future work.

A role for C207 in catalytic turnover of SO has been proposed by Enemark and co-workers,<sup>25</sup> who suggest that

(21) George, G. N.; Garrett, R. M.; Graf, T.; Prince, R. C.; Rajagopalan, K. V. *J. Am. Chem. Soc.* **1998**, *120*, 4522–4523.

(22) Pacheco, A.; Basu, P.; Borbat, P.; Raitsimring, A. M.; Enemark, J. H. *Inorg. Chem.* **1996**, *35*, 7001–7008.

(23) We note that EXAFS analysis cannot readily distinguish between scatterers of similar atomic number, such as chlorine and sulfur, or nitrogen and oxygen (e.g., ref 24).

**Table 1.** EXAFS Curve-Fitting for Different Oxidation States of C207S Sulfite Oxidase<sup>a</sup>

| oxidation state | interaction       | <i>N</i> | <i>R</i> (Å) | $\sigma^2$ (Å <sup>2</sup> ) | $\Delta E_0$ (eV) | <i>F</i> |
|-----------------|-------------------|----------|--------------|------------------------------|-------------------|----------|
| Mo(VI)          | Mo=O              | 3        | 1.749(2)     | 0.0039(1)                    | -16.8(7)          | 0.2674   |
|                 | Mo-S              | 2        | 2.475(3)     | 0.0041(2)                    |                   |          |
| Mo(V)           | Mo=O              | 1        | 1.698(4)     | 0.0026(4)                    | -18.5(8)          | 0.31457  |
|                 | Mo-S              | 2        | 2.368(3)     | 0.0028(2)                    |                   |          |
|                 | Mo-O              | 2        | 1.964(4)     | 0.0050(5)                    |                   |          |
| Mo(IV)          | Mo=O              | 1        | 1.699(5)     | 0.0028(2)                    | -18.6(13)         | 0.3524   |
|                 | Mo-S              | 2        | 2.339(6)     | 0.0021(2)                    |                   |          |
|                 | Mo-O <sup>b</sup> | 1        | 2.184(41)    | 0.0049(3)                    |                   |          |
|                 | Mo-O <sup>b</sup> | 1        | 2.053(21)    | 0.0038(3)                    |                   |          |

<sup>a</sup> Coordination numbers *N*, interatomic distances *R* are given in Å, Debye-Waller factors  $\sigma^2$  (the mean-square deviations in interatomic distance) are given in Å<sup>2</sup>, and the threshold energy shifts  $\Delta E_0$  are given in eV. The values in parentheses are the estimated standard deviations obtained from the diagonal elements of the covariance matrix. The fit-error function *F* is defined as  $\sqrt{k^6 \sum (\chi_{\text{calc}} - \chi_{\text{expt}})^2 / \sum \chi_{\text{expt}}^2}$ , where the summation is over all data points included in the refinement. <sup>b</sup> The fit was improved somewhat by including two different Mo-O interactions, as opposed to a single interaction (*F* = 0.3524 vs 0.3744). Because of the high mutual correlation observed for  $\sigma^2$  for the two Mo-O factors, these were restrained in the refinement and floated as a single variable so that  $\sigma^2$  varied proportionally to the difference in *R*.

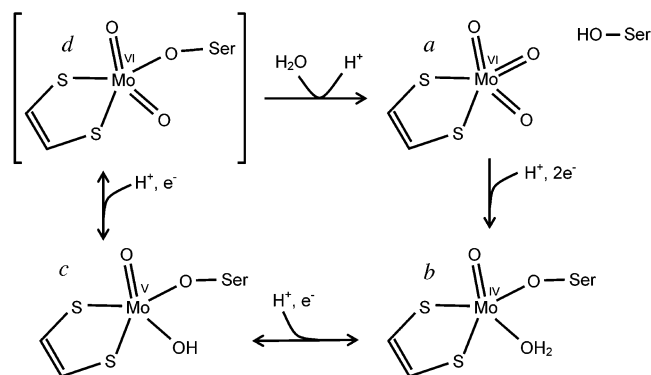


**Figure 7.** Proposed structures of the C207S active site: (a) the tri-oxo active site of as-isolated C207S enzyme, (b) the reduced form generated at low redox potentials, and (c) a hypothetical Mo(VI) dioxo site which loses the serine ligand to regenerate (a). We note that, for (b), (c), and (d), the overall charge of the site is  $-1$ , but that for (a) is  $-2$ .

the O=Mo-S-C dihedral angle, which is observed crystallographically to be close to  $180^\circ$ , causes a high degree of covalency in the Mo-S(Cys) bond. This in turn may be important in facilitating preferential transfer of one Mo=O to sulfite during catalysis, and in fine-tuning the redox

potentials of the active site.<sup>25,26</sup> Plant nitrate reductases are closely related to sulfite oxidases, and we have previously shown that structural changes in the Mo-S coordination of oxidized Mo(VI) enzyme are induced by catalytic turnover.<sup>27</sup> These changes were manifest as a lower Mo-S EXAFS amplitude in nitrate reductase prior to catalytic turnover, relative to that observed in sulfite oxidase and in nitrate reductase immediately following catalytic turnover. EXAFS curve-fitting suggested that the Mo-S coordination number did not change, but that the decreased amplitude was due to a higher Mo-S Debye-Waller factor for the enzyme prior to turnover, indicating the presence of a distribution in Mo-S bond lengths. This was interpreted as increased Mo=O trans-effects for one of the sulfurs arising from conformational change, although dissociation of one sulfur ligand to the metal could not be excluded.<sup>27</sup> The data presented here suggest that with C207S sulfite oxidase a serine in position 207 is labile and can reversibly bind molybdenum. There is no evidence that C207 can perform similar chemistry, but the lability of S207 may be related to active site conformational flexibility of the sort previously suggested for nitrate reductases,<sup>27</sup> perhaps involving dynamic changes to C207 conformation during the catalytic cycle.

**Acknowledgment.** Parts of this work were carried out at the Stanford Synchrotron Radiation Laboratory (SSRL), a national user facility operated by Stanford University on behalf of the U.S. Department of Energy, Office of Basic Energy Sciences. The SSRL Structural Molecular Biology Program is supported by the Department of Energy, Office of Biological and Environmental Research, and by the National Institutes of Health, National Center for Research Resources, Biomedical Technology Program. Work at the University of Saskatchewan was supported by a Canada Research Chair award (G.N.G.), the University of Saskatchewan, the Province of Saskatchewan, the National Science and Engineering Research Council (Award #283315), the National Institutes of Health (GM57375), the Canadian Institute for Health Research, and the Canada Foundation for Innovation (Award #201742). Work at Duke University was supported by NIH grant GM44283.

IC0489847

- (24) George, G. N.; Kipke, C. A.; Prince, R. C.; Sunde, R. A.; Enemark, J. H.; Cramer, S. P. *Biochemistry* **1989**, *28*, 5075-5080.  
 (25) Izumi, Y.; Glaser, T.; Rose, K.; McMaster, J.; Basu, P.; Enemark, J. H.; Hedman, B.; Kodgson, K. O.; Solomon, E. I. *J. Am. Chem. Soc.* **1999**, *121*, 10035-10046.

- (26) Note that, because these workers used a different method of energy calibration than we used in our earlier work, the covalency of the Mo-S(Cys207) bond is overstated.  
 (27) George, G. N.; Mertens, J. A.; Campbell, W. H. *J. Am. Chem. Soc.* **1999**, *121*, 9730-9731.